

CO<sub>2</sub> hydrogenation to methanol on tungsten-doped Cu/CeO<sub>2</sub> catalysts

Yong Yan<sup>a,b</sup>, Roong Jien Wong<sup>a,b,c</sup>, Zhirui Ma<sup>d</sup>, Felix Donat<sup>e</sup>, Shibo Xi<sup>f</sup>, Syed Saqine<sup>a,b,c</sup>, Qianwenhao Fan<sup>a,b</sup>, Yonghua Du<sup>f,g</sup>, Armando Borgna<sup>f</sup>, Qian He<sup>h</sup>, Christoph R. Müller<sup>e</sup>, Wei Chen<sup>d</sup>, Alexei A. Lapkin<sup>b,i</sup>, Wen Liu<sup>a,b,\*</sup>

<sup>a</sup> School of Chemical and Biomedical Engineering, Nanyang Technological University, 62 Nanyang Drive, Singapore 637459, Singapore

<sup>b</sup> Cambridge Centre for Advanced Research and Education, 1 Create Way, #05-05, Singapore 138602, Singapore

<sup>c</sup> Nanyang Environmental and Water Research Institute, Nanyang Technological University, 1 Cleantech Loop, Singapore 637141, Singapore

<sup>d</sup> Department of Chemistry, National University Singapore, 3 Science Drive 3, Singapore 117543, Singapore

<sup>e</sup> Department of Mechanical and Process Engineering, ETH Zurich, Leonhardstrasse 21, 8092 Zürich, Switzerland

<sup>f</sup> Institute of Chemical and Engineering Sciences, Agency for Science, Technology and Research, 1 Pesek Road, Singapore 627833, Singapore

<sup>g</sup> Brookhaven National Laboratory, National Synchrotron Light Source II, Bldg. 743, P.O. Box 5000, Upton, NY 11973-5000, United States

<sup>h</sup> Department of Materials Science and Engineering, National University Singapore, 9 Engineering Drive 1, Singapore 117575, Singapore

<sup>i</sup> Department of Chemical Engineering and Biotechnology, University of Cambridge, Philippa Fawcett Drive, Cambridge CB3 0AS, United Kingdom

## ARTICLE INFO

## Keywords:

CO<sub>2</sub>  
Methanol  
Oxygen vacancy  
Hydrogenation  
Ceria  
Metal-support interface

## ABSTRACT

The catalytic hydrogenation of CO<sub>2</sub> to methanol depends significantly on the structures of metal-oxide interfaces. We show that doping a high-valency metal, viz. tungsten, to CeO<sub>2</sub> could render improved catalytic activity for the hydrogenation of CO<sub>2</sub> on a Cu/CeW<sub>0.25</sub>O<sub>x</sub> catalyst, whilst making it more selective towards methanol than the undoped Cu/CeO<sub>2</sub>. We experimentally investigated and elucidated the structural-functional relationship of the Cu/CeO<sub>2</sub> interface for CO<sub>2</sub> hydrogenation. The promotional effects are attributed to the irreversible reduction of Ce<sup>4+</sup> to Ce<sup>3+</sup> by W-doping, the suppression of the formation of redox-active oxygen vacancies on CeO<sub>2</sub>, and the activation of the formate pathway for CO<sub>2</sub> hydrogenation. This catalyst design strategy differs fundamentally from those commonly used for CeO<sub>2</sub>-supported catalysts, in which oxygen vacancies with high redox activity are considered desirable.

## 1. Introduction

Carbon capture, storage and utilisation (CCSU) is a scheme that complements the transition to renewable energies and electrification towards building a low-carbon economy [1–4]. An important aspect of CCSU is to synthesise, at large scale, chemicals and fuels from captured CO<sub>2</sub> [5,6]. Amongst the various CO<sub>2</sub>-derived products, methanol is a highly attractive target, owing to its versatile roles as a gateway molecule and a liquid fuel substitute [7–10]. Recent analyses have shown that methanol synthesised from captured CO<sub>2</sub> and renewable hydrogen has a significantly lower environmental impact than that produced from natural gas or coal [11]. Furthermore, the use of methanol as a fuel additive could substantially reduce CO<sub>2</sub> emission from vehicle exhaust [12].

To date, there is limited commercial processes that produces methanol from CO<sub>2</sub> [13,14], partly because the commercial Cu/ZnO/Al<sub>2</sub>O<sub>3</sub> methanol synthesis catalysts are insufficiently stable under the CO<sub>2</sub>

hydrogenation conditions [15,16]. Meanwhile, several catalysts with promising performance have been developed and evaluated at pilot scales [17–23]. Significant experimental and theoretical research have been conducted to establish reaction pathways of methanol synthesis. It is generally understood that the activation of CO<sub>2</sub> is the first rate-limiting step. Depending on the nature of the active sites, CO<sub>2</sub> may form formate (HCOO\*), carboxyl (\*COOH), carbonate (\*CO<sub>3</sub>), bicarbonate (\*HCO<sub>3</sub>), or a surface carbonyl (\*CO) upon adsorption [24,25]. The further hydrogenation of the surface intermediates; e.g. HCOO\* and \*CO, is regarded as the second rate-limiting step [25,26]. This is followed by the successive hydrogenation to form \*CH<sub>3</sub>O, the hydrogenation and desorption of which is the final step to methanol production. According to the second rate-limiting step, the reaction mechanisms are classified as (i) the formate pathway, where HCOO\* is a key reaction intermediate, or (ii) the reverse water-gas-shift (RWGS) pathway, where \*COOH or \*CO are key reaction intermediates [25]. However, the identities of the active sites of many high-performing catalysts remain

\* Corresponding author at: School of Chemical and Biomedical Engineering, Nanyang Technological University, 62 Nanyang Drive, Singapore 637459, Singapore.  
E-mail address: [wenliu@ntu.edu.sg](mailto:wenliu@ntu.edu.sg) (W. Liu).

<https://doi.org/10.1016/j.apcatb.2022.121098>

Received 21 October 2021; Received in revised form 16 December 2021; Accepted 12 January 2022

Available online 14 January 2022

0926-3373/© 2022 Elsevier B.V. All rights reserved.

debatable and the structural-functional relationships at the metal-oxide interfaces are yet to be fully understood [13,16,27–29]. For any metal/oxide interface catalysts, closing these knowledge gaps will enable the rapid improvement of catalyst design.

Amongst the various Cu-based catalysts, Cu/CeO<sub>2</sub> is known to catalyse methanol synthesis via the RWGS pathway, where CO is produced as a reaction intermediate as well as a byproduct. However, unmodified Cu/CeO<sub>2</sub> shows relatively low activity (space time yield, STY < 2 mol<sub>MeOH</sub>·kg<sub>cat</sub><sup>−1</sup>·h<sup>−1</sup>) and moderate selectivity (~50%) [30,31]. Attempts to improve the activities of CeO<sub>2</sub>-based catalysts often evolve around promoting their redox activity, e.g. by preparing morphologically well-defined CeO<sub>2</sub> supports with high redox activities [32,33] or doping lower-valency cations (e.g. Co<sup>3+</sup> and Pr<sup>3+</sup>) to generate additional oxygen vacancies [34–38]. These approaches invariably promote RWGS and the formation of CO, whose adsorption on Cu is weak, therefore limiting the overall methanol productivity and selectivity [39–41].

According to recent studies [35,42], doping high-valency metals such as Mo and W will reduce CeO<sub>2</sub> as the dopants donate electrons to adjacent Ce<sup>4+</sup>. Such reduction does not involve the generation of additional oxygen vacancies and is therefore fundamentally different from the conventional reduction by lattice oxygen removal. Therefore, this doping effect offers an alternative approach to modify the activity of Cu/CeO<sub>2</sub> without generating additional oxygen vacancies [43]. Here, we successfully prepared a W-doped Cu/CeO<sub>2</sub> catalyst, viz. Cu/CeW<sub>0.25</sub>O<sub>x</sub>, which shows a substantially enhanced methanol activity (CO<sub>2</sub> conversion = 13%, STY = 12.32 mol<sub>MeOH</sub>·kg<sub>cat</sub><sup>−1</sup>·h<sup>−1</sup>) over unmodified Cu/CeO<sub>2</sub> (CO<sub>2</sub> conversion = 1.3%, STY = 1.26 mol<sub>MeOH</sub>·kg<sub>cat</sub><sup>−1</sup>·h<sup>−1</sup>) at 250 °C, 35 bar total pressure and a weight hourly space velocity (WHSV) of 15000 mL g<sub>cat</sub><sup>−1</sup> h<sup>−1</sup>. The Cu/CeW<sub>0.25</sub>O<sub>x</sub> catalyst is also significantly more selective towards methanol (87% vs. 51%) than the undoped Cu/CeO<sub>2</sub>. In fact, the activity of Cu/CeW<sub>0.25</sub>O<sub>x</sub> is on par with some of the best performing Cu-based CO<sub>2</sub>-to-methanol catalysts reported in the literature [44–51]. In situ vibrational spectroscopy and in situ X-ray scattering experiments were conducted to elucidate the roles of different types of Ce<sup>3+</sup> sites and oxygen vacancies during methanol synthesis.

## 2. Experimental

### 2.1. Catalyst preparation

All chemicals were purchased from Sigma Aldrich and used as received without further purification. To prepare W-doped CeO<sub>2</sub>, urea was added into an aqueous Ce(NO<sub>3</sub>)<sub>3</sub> solution (0.005 M) at a urea: Ce<sup>3+</sup> ratio of 10: 1. Then, (NH<sub>4</sub>)<sub>6</sub>H<sub>2</sub>W<sub>12</sub>O<sub>40</sub>·xH<sub>2</sub>O (at a W: Ce ratio of 1: 4), together with equal mass of H<sub>2</sub>C<sub>2</sub>O<sub>4</sub>·2H<sub>2</sub>O, was dissolved in the same solution. Subsequently, the solution was transferred into an autoclave, which was sealed and heated to 150 °C to react for 12 h. The resulting precipitate was filtered and washed with deionized water, dried at 100 °C overnight, and calcined at 500 °C for 1 h in air. Undoped CeO<sub>2</sub> was prepared by a similar procedure, but without (NH<sub>4</sub>)<sub>6</sub>H<sub>2</sub>W<sub>12</sub>O<sub>40</sub>·xH<sub>2</sub>O and H<sub>2</sub>C<sub>2</sub>O<sub>4</sub>·2H<sub>2</sub>O.

Supported Cu catalysts were prepared by wet impregnation. In a typical preparation, the support material (CeO<sub>2</sub> or W-doped CeO<sub>2</sub>) was added to an aqueous solution containing required amount of Cu(NO<sub>3</sub>)<sub>2</sub> under rigorous stirring. The targeted Cu loading was 10 wt%. After impregnation, the excess water was removed in a rotary evaporator at 80 °C. The catalysts were obtained by drying the resulting solid at 80 °C in air for 12 h, followed by calcination at 500 °C in air for 2 h.

### 2.2. Ex situ sample characterisation

The crystalline structural information was investigated by powder X-ray diffraction (XRD) on a Bruker AXS D8 diffractometer with Cu K $\alpha$  radiation ( $\lambda$  = 1.5406 Å) at 40 kV and 40 mA. The morphology of the catalysts was examined by high-resolution transmission electron microscopy (HRTEM) using a JEOL JEM 2100F TEM, working at an

accelerating voltage of 200 kV. The N<sub>2</sub> adsorption-desorption isotherms were measured on a Micromeritics 3 flex instrument at −196 °C. Prior to N<sub>2</sub> physisorption, all samples were degassed at 180 °C for 5 h in vacuum. The specific surface areas were calculated according to the Brunauer-Emmett-Teller (BET) equation using the data over the  $P/P_0$  range from 0.05 to 0.35. The X-ray photoelectron spectra (XPS) of the catalysts were acquired on a Kratos Axis Supra spectrophotometer with a dual anode monochromatic K $\alpha$  excitation source. All binding energies were calibrated against the adventitious carbon C 1s peak at 284.8 eV. Cu speciation was determined from the Auger electron spectroscopy with XPS [52,53].

Inductively coupled plasma optical emission spectroscopy (ICP-OES, Agilent 5100 VDV) was used to quantify the mass fractions of Cu, Ce, and W elements in the catalysts.

H<sub>2</sub> temperature-programmed reduction (H<sub>2</sub>-TPR) measurements were carried out on a Micromeritics Autochem II 2920 instrument. Firstly, the catalysts were loaded into a quartz U-tube reactor and pre-treated under an air flow (50 mL min<sup>−1</sup>) at 500 °C for 60 min, followed by cooling to 35 °C in He. After 30 min, 5% H<sub>2</sub>/N<sub>2</sub> (50 mL min<sup>−1</sup>) was passed through the catalyst bed until a stable thermal conductivity detector (TCD) signal was observed. Subsequently, the temperature was increased from 35 °C to 1000 °C at a constant rate of 10 °C min<sup>−1</sup> in 5% H<sub>2</sub>/N<sub>2</sub>. The outlet gas, after H<sub>2</sub>O removal, was analysed by the TCD to quantify the consumption of H<sub>2</sub> during the TPR.

CO<sub>2</sub> temperature-programmed desorption (CO<sub>2</sub>-TPD) was performed on the same Autochem II 2920 instrument equipped with a MKS Cirrus II mass spectrometer (MS). The total gas flow rate through the catalyst bed was kept constant at 50 mL min<sup>−1</sup>. Prior to each TPD experiment, the sample (~100 mg) was pretreated in 5% H<sub>2</sub>/N<sub>2</sub> at 500 °C for 60 min and cooled to 35 °C in He. At 35 °C, the sample was exposed to 10% CO<sub>2</sub>/He for 60 min, followed by He purging for 30 min. Then, the temperature was raised to 500 °C at a ramping rate of 10 °C min<sup>−1</sup>, whilst the mass spectrometer analysed the outlet gas and recorded the signals of CO ( $m/z$  = 28) and CO<sub>2</sub> ( $m/z$  = 44).

The surface dispersion of Cu metals was quantified by N<sub>2</sub>O chemisorption measurements on a Micromeritics Autochem II 2920 instrument. In a typical measurement, Cu was first reduced in 10% H<sub>2</sub>/Ar prior to N<sub>2</sub>O chemisorption, followed by a second H<sub>2</sub> reduction step to remove the chemisorbed oxygen. H<sub>2</sub> reduction was first performed at 300 °C for 60 min. After cooling to room temperature, 10% N<sub>2</sub>O/He was introduced to the sample until N<sub>2</sub>O consumption was no longer observed. Hydrogen reduction, following the H<sub>2</sub>-TPR programme described above, was then conducted to quantify the amount of surface Cu atom based on the amount of H<sub>2</sub> consumed.

### 2.3. CO<sub>2</sub> hydrogenation to methanol

The performance of the catalyst was examined in a fixed-bed reactor. Before CO<sub>2</sub> hydrogenation, the loaded catalysts were reduced in situ in 50 mL min<sup>−1</sup> of 10% H<sub>2</sub>/He at 500 °C and 10 bar for 60 min. In each experiment, 200 mg of catalyst was used to convert a 23:69:8 mixture of CO<sub>2</sub>, H<sub>2</sub> and N<sub>2</sub>, with a total flow rate of 50 mL min<sup>−1</sup> (STP) at 250 °C and 35 bar total pressure. Using N<sub>2</sub> as an internal standard, the composition of outlet gas was analysed by online gas chromatography (Agilent 7890B) equipped with both flame ionisation detector (FID) detector and TCD detector. Condensation of the liquid products was avoided by trace heating the gas sampling line to 90 °C. Kinetics data were collected by measuring the rate when the CO<sub>2</sub> conversion was below 10%.

### 2.4. In situ catalyst characterisation

In situ diffuse reflectance infrared Fourier transform spectroscopy (DRIFTS) was carried out on a Bruker Tensor II FTIR spectrometer. The FTIR was equipped with a liquid-N<sub>2</sub> cooled MCT/A detector, a Pike DiffuseIR accessory, and a high-pressure reaction cell. Prior to each

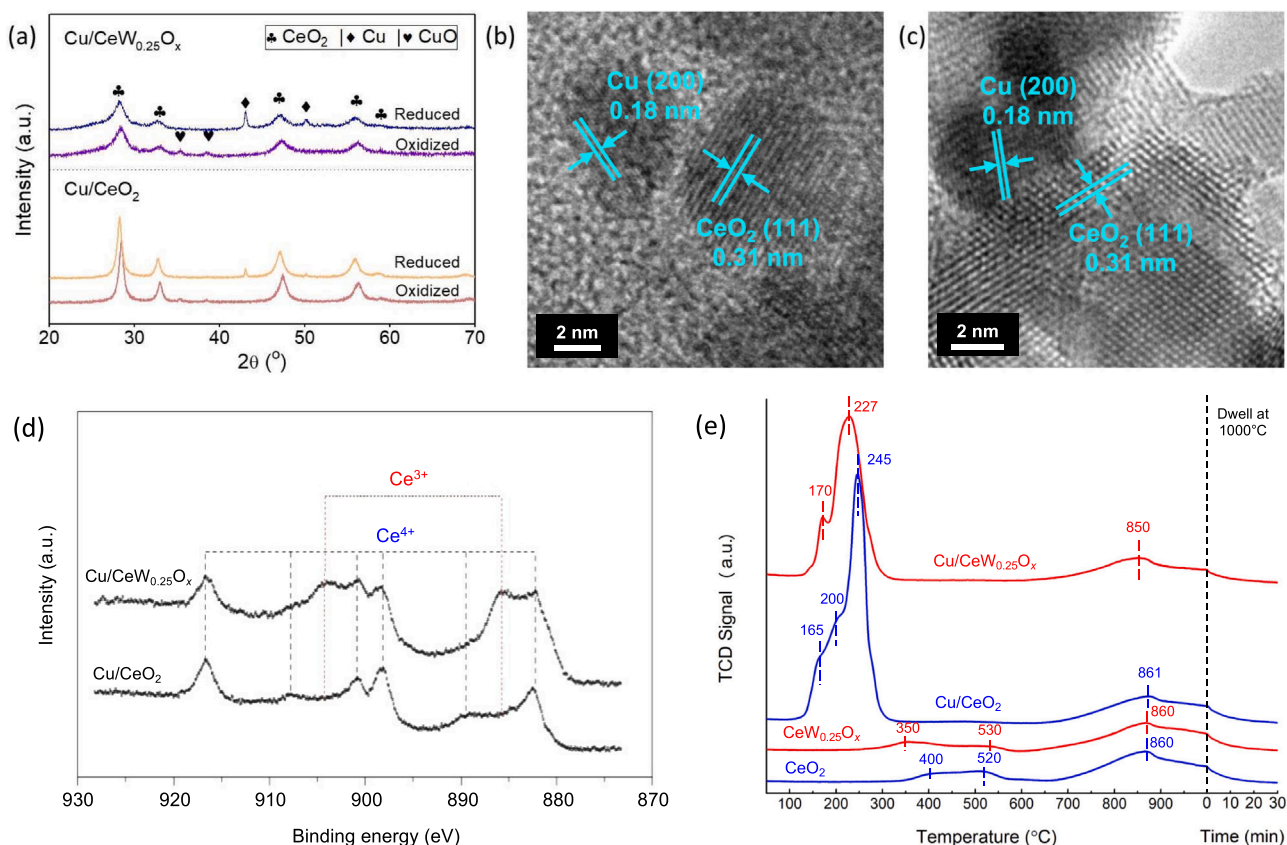


**Fig. 1.** Ex situ characterisation of the as-prepared supports and Cu-loaded catalysts. (a): XRD patterns of the reduced and the oxidised catalysts. (b) and (c): HRTEM images of Cu/CeO<sub>2</sub> and Cu/CeW<sub>0.25</sub>O<sub>x</sub>, respectively. (d) High-resolution XPS spectra of Ce 3d. (e) H<sub>2</sub>-TPR profiles of the air-calcined bare catalyst supports and the Cu loaded catalysts.

experiment, the sample was reduced in 50 mL min<sup>-1</sup> of 10% H<sub>2</sub>/He at 500 °C for 60 min and cooled in He to the desired reaction temperature (250 °C). The background spectrum was collected in He, at the reaction temperature. Each spectrum was obtained by averaging over 100 consecutive scans, each with a spectral resolution of 4 cm<sup>-1</sup>.

In situ X-ray absorption spectra (XAS) were measured using wafer samples (I.D. 10 mm pellets) in a customised high pressure reaction cell equipped with two beryllium windows at the XAFCA beamline of Singapore Synchrotron Light Source (SSLS). The beamline has a flux of  $1.6 \times 10^{10}$  photons per second at 7 keV. A Si(111) crystal was used as the monochromator for the energy range from 2.1 to 12.8 keV. The typical scan time was about 20 min. The data were processed using IFEFFIT software packages. XAS of the as-prepared samples were measured at RT under He purging. The spectra of the reduced samples were collected after reduction in 10% H<sub>2</sub>/He at 500 °C, 10 bar total pressure, for 60 min. In situ measurements were carried out when the samples were exposed to a 3:1 mixture of H<sub>2</sub> and CO<sub>2</sub> at 250 °C and 10 bar.

Near ambient pressure X-ray photoelectron spectroscopy (NAP-XPS) experiments were performed in a multichambered Specs system equipped with an Al/Mg twin anode X-ray source and a Phoibos hemispherical energy analyzer. A residual gas analyzer (RGA) was connected to the NAP lens chamber, which was exposed to 0.1–1 mbar of reaction gas, supplied through a 300 μm nozzle. The NAP cell was degassed before each experiment by heating to 627 °C under vacuum until the chamber pressure fell below  $1 \times 10^{-9}$  mbar. In each NAP-XPS experiment, the catalyst was first reduced in 0.4 mbar H<sub>2</sub> at 500 °C, followed by oxidation in 0.5 mbar CO<sub>2</sub> at RT. Then, 0.3 mbar CO<sub>2</sub> and 0.9 mbar H<sub>2</sub> were fed into the measurement chamber at 250 °C to simulate a CO<sub>2</sub> hydrogenation environment. Finally, the samples were oxidised in 0.4 mbar O<sub>2</sub> at 500 °C. NAP-XPS spectra were collected at each segment of the experiment, when the samples were believed to have reached steady

state.

### 3. Results and discussion

#### 3.1. Characterisation of the as-prepared catalysts

Fig. 1 presents the characterisation of the as-synthesised CeO<sub>2</sub> supports and the Cu/CeO<sub>2</sub> catalysts, with and without W-doping. Prior to Cu loading, the X-ray diffraction (XRD) patterns of both the unmodified and the W-doped CeO<sub>2</sub> can be fully indexed by the fluorite-structured CeO<sub>2</sub> phase (Fig. S1). After Cu loading, the freshly calcined catalysts show diffraction peaks of CuO, which changed to Cu after H<sub>2</sub> reduction (Fig. 1a). In all cases, the absence of any diffraction peak associated with WO<sub>x</sub> species suggests that W atoms are finely dispersed on and, or in the CeO<sub>2</sub> support. In addition, the samples containing W-doped CeO<sub>2</sub> show greater extent of peak broadening than the samples without W. This additional peak broadening effect is attributed to the additional microstrain (e.g. the presence of defects) that is commonly observed in metal-doped CeO<sub>2</sub> [54–58]. The lattice parameters of CeO<sub>2</sub> in the oxidised Cu/CeO<sub>2</sub> and Cu/CeW<sub>0.25</sub>O<sub>x</sub> catalysts were estimated by Rietveld refinement of the diffraction patterns to be  $5.41 \pm 0.01$  and  $5.44 \pm 0.01$  Å, respectively. The increase in the lattice parameter of CeO<sub>2</sub> upon W-doping signifies the reduction of Ce<sup>4+</sup> to Ce<sup>3+</sup> [59]. In fact, both the reduced and oxidised forms of Cu/CeW<sub>0.25</sub>O<sub>x</sub> show larger CeO<sub>2</sub> lattices than the Cu/CeO<sub>2</sub> sample, suggesting the reduction of Ce<sup>4+</sup> to Ce<sup>3+</sup> by W doping is ubiquitous in all the chemical environments of interest. The HRTEM images, depicted in Fig. 1b and c, show that both catalysts consist of grains of Cu and CeO<sub>2</sub> of ~4 nm and ~5 nm in size, respectively. The HRTEM observations further support the conclusion that the additional peak broadening of the W-doped CeO<sub>2</sub> observed in Fig. 1a is due to increased microstrain rather than decreased grain sizes of CeO<sub>2</sub>.

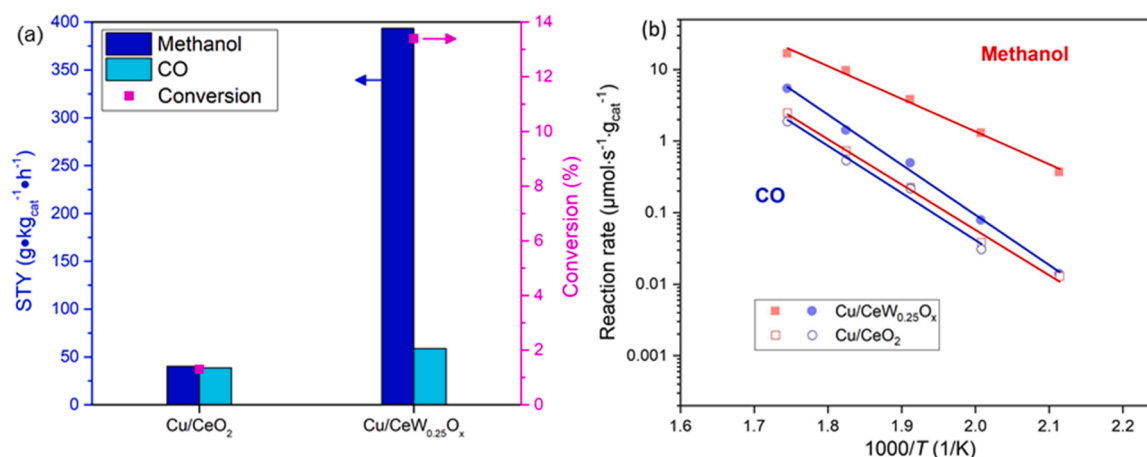


**Fig. 2.** (a) Methanol STY and CO<sub>2</sub> conversion over Cu/CeO<sub>2</sub> and Cu/CeW<sub>0.25</sub>O<sub>x</sub> in a 23:69:8 mixture of CO<sub>2</sub>/H<sub>2</sub>/N<sub>2</sub> at 250 °C, 35 bar total pressure, with WHSV of 15,000 mL g<sub>cat</sub><sup>-1</sup> h<sup>-1</sup>. The error bars for methanol selectivity, calculated based on the data variability during the 72 h TOS experiments, are too small to be shown. (b) Arrhenius plots of the rate of CO and methanol formation over the Cu/CeO<sub>2</sub> and Cu/CeW<sub>0.25</sub>O<sub>x</sub> catalysts under the same operating conditions as (a), except the varied reaction temperatures.

The lattice fringes of 0.18 nm and 0.31 nm observed in the HRTEM images correspond to the Cu(200) and CeO<sub>2</sub>(111) planes, respectively. Supplementary HRTEM images, including lower magnification ones, are provided in Fig. S2 of Supporting Information. The identification of the CeO<sub>2</sub> grains were further confirmed by selected area electron diffraction (SAED) analysis, as shown Fig. S2c and d. It should be noted that the resolution of the present HRTEM analysis is not sufficiently high to verify the lattice expansion due to W-doping (as suggested by the XRD results). The actual Cu loadings on Cu/CeO<sub>2</sub> and Cu/CeW<sub>0.25</sub>O<sub>x</sub>, as determined by ICP-OES (Table S1), are 9.8 wt% and 10.9 wt%, respectively. The specific surface areas of the Cu/CeO<sub>2</sub> and Cu/CeW<sub>0.25</sub>O<sub>x</sub> catalysts, as determined by the BET analysis of the N<sub>2</sub> adsorption-desorption isotherms, are 105 and 84 m<sup>2</sup>g<sup>-1</sup>, respectively. Given the lack of contrast of Cu on CeO<sub>2</sub> in TEM, the dispersion of Cu on the Cu/CeO<sub>2</sub> and Cu/CeW<sub>0.25</sub>O<sub>x</sub> catalysts is estimated by N<sub>2</sub>O chemisorption (results shown in Fig. S3), to be around 16.8% and 16.9%, respectively. Care is taken to discriminate the chemisorption signals associated with Cu and CeO<sub>2</sub>. These dispersion values translate to mean Cu particle sizes of ~4.3 nm, assuming uniform particle sizes and spherical particle shape. The estimated particle sizes agree with the HRTEM (Fig. 1b and c), which show Cu particles of 4–5 nm in size. Therefore, despite the marginal increase in Cu loading and decrease in BET surface area, W-doping appears to have negligible effect on the morphology and dispersion of the supported Cu particles.

The chemical states of the surface regions of the catalysts were probed by XPS. The Ce 3d XPS spectra, shown in Fig. 1d, reflect the ratio of Ce<sup>3+</sup> to Ce<sup>4+</sup> in the surface region of the catalysts. On Cu/CeO<sub>2</sub>, the major XPS peaks are assigned to a doublet of Ce<sup>4+</sup> with an orbital splitting of ~18.6 eV, accompanied by the shakedown features of one or two electron transfer from a filled O 2p orbital to an empty Ce 4f orbital [60]. The doublet corresponding to Ce<sup>3+</sup> is significantly more intense in the spectra of the Cu/CeW<sub>0.25</sub>O<sub>x</sub> than that of Cu/CeO<sub>2</sub>, indicating that the reduction of Ce<sup>4+</sup> by W was not only a bulk phenomenon, but also profound near the surface. The consequence of W-doping on the states of Cu at the Cu/oxide interfaces is analysed by Cu AES, as shown in Fig. S4a. Looking at the quantitative analyses of the fitted Cu Auger peaks, as shown in Fig. S4b, W-doping does not cause any significant change to the amount of Cu<sup>+</sup> in the surface region, where Cu<sup>+</sup> is regarded as the Cu species at the Cu/oxide interfaces [52].

The reducibility of the air-calcined CeO<sub>2</sub> support and the Cu-loaded catalysts are investigated by H<sub>2</sub>-TPR, as shown in Fig. 1e. Three types of TPR peaks can be seen. Firstly, the low temperature peaks (< 200 °C) correspond to the reduction of CuO to metallic Cu [61]. Secondly, the intermediate temperature (200–600 °C) peaks are assigned to the

removal of oxygen from the surface of the CeO<sub>2</sub> supports [62]. Lastly, the high temperature peaks (> 600 °C) can be assigned to the removal of bulk lattice oxygen from CeO<sub>2</sub> [63]. After Cu loading, the intermediate-temperature TPR peaks (350–530 °C) associated with the reduction of surface CeO<sub>2</sub> shift to lower temperatures, showing intense peaks around 227–245 °C, probably because Cu catalyses the reduction of CeO<sub>2</sub> by facilitating hydrogen spill-over. Upon W-doping, the main TPR peak associated with the removal of lattice oxygen from the surface of the fully oxidised CeO<sub>2</sub>, shifts from 245 °C (in the case of Cu/CeO<sub>2</sub>) to 227 °C (for Cu/CeW<sub>0.25</sub>O<sub>x</sub>), suggesting that the addition of W might have promoted the catalyst's ability to activate H<sub>2</sub>. Although Cu/CeW<sub>0.25</sub>O<sub>x</sub> has substantially higher Ce<sup>3+</sup> concentration, its overall reducibility, as shown by the total areas of the TPR peaks, does not appear significantly different from Cu/CeO<sub>2</sub>; this observation agrees with the catalyst design hypothesis outlined in the Introduction.

### 3.2. CO<sub>2</sub> hydrogenation performance and mechanism

As shown in Fig. 2, the CO<sub>2</sub> hydrogenation activity of Cu/CeW<sub>0.25</sub>O<sub>x</sub>, evaluated at 250 °C and 35 bar, in a 23:69:8 mixture of CO<sub>2</sub>:H<sub>2</sub>:N<sub>2</sub>, was substantially higher and more selective towards methanol than the unmodified Cu/CeO<sub>2</sub>. On average, the unmodified Cu/CeO<sub>2</sub> showed a space-time yield (STY) of 1.26 mol<sub>MeOH</sub>·kg<sub>cat</sub><sup>-1</sup>·h<sup>-1</sup>, a CO<sub>2</sub> conversion of 1.3% and a methanol selectivity of 51%. The STY of the Cu/CeO<sub>2</sub> catalyst is comparable to the other Cu/CeO<sub>2</sub>-type catalysts reported in the literature (i.e. with STY varying in the range of 0.6–2.9 mol<sub>MeOH</sub>·kg<sub>cat</sub><sup>-1</sup>·h<sup>-1</sup>), as shown in Table S2. In contrast, the Cu/CeW<sub>0.25</sub>O<sub>x</sub> catalysts exhibited a one order of magnitude increase in STY (12.3 mol<sub>MeOH</sub>·kg<sub>cat</sub><sup>-1</sup>·h<sup>-1</sup>), as well as significantly improved CO<sub>2</sub> conversion and methanol selectivity of 13% and 87%, respectively. The standard errors of the mean STY and mean selectivity, estimated over 72 h time-on-stream (TOS, see Fig. S5) were both well below 1%. Given that Cu/CeO<sub>2</sub> and Cu/CeW<sub>0.25</sub>O<sub>x</sub> have comparable specific surface areas (105 and 84 m<sup>2</sup>g<sup>-1</sup>, respectively), Cu loadings (9.8 wt% and 10.9 wt%, respectively), Cu chemical states (see AES in Fig. S4), Cu dispersion (see Table S1), and Cu particle sizes, such significant improvement in methanol synthesis activity of the Cu/CeW<sub>0.25</sub>O<sub>x</sub> catalyst over Cu/CeO<sub>2</sub> can only be explained by changes in the catalytic structure and, or possibly a change in the dominating reaction pathway. Additionally, the Cu/CeO<sub>2</sub> and Cu/CeW<sub>0.25</sub>O<sub>x</sub> catalysts showed stable performances over 72 h TOS (Fig. S5), suggesting satisfactory stabilities. In comparison, we note that a Cu/WO<sub>3</sub> catalyst (results not shown) prepared by impregnating 10 wt% Cu on WO<sub>3</sub> showed no detectable CO<sub>2</sub> hydrogenation activity at 250 °C and 35 bar, suggesting that the Cu/WO<sub>3</sub> interfaces,

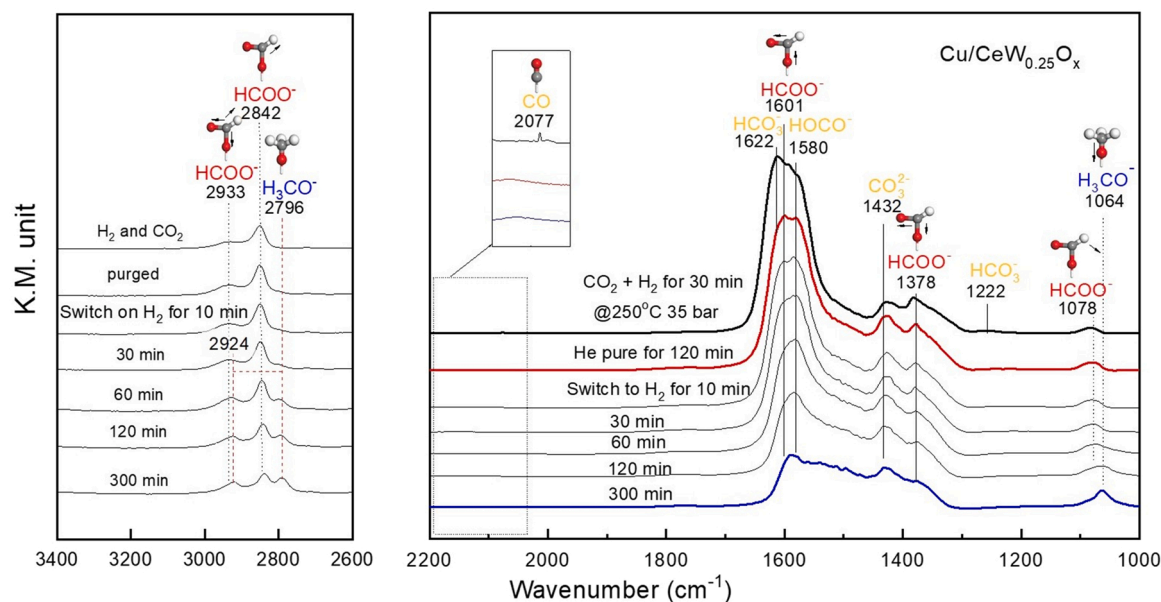


**Fig. 3.** DRIFTS spectra recorded over Cu/CeW<sub>0.25</sub>O<sub>x</sub> when the catalyst was exposed to CO<sub>2</sub> hydrogenation conditions for 30 min, followed by He purging for 120 min, and then treated with H<sub>2</sub> only. All measurements were performed at 35 bar total pressure at 250 °C.

even if it was present on Cu/CeW<sub>0.25</sub>O<sub>x</sub>, was not responsible for the observed catalytic enhancement.

Arrhenius analyses of the apparent rates of formation of methanol and CO are shown in Fig. 2b. All rate measurements were taken under differential reactor conditions, in which the catalyst weight and total flow rate were adjusted accordingly to keep the CO<sub>2</sub> conversion below 10%. For Cu/CeO<sub>2</sub>, the apparent activation energies of the formation of CO and methanol are similar, i.e.  $\sim 55 \text{ kJ} \pm 5 \text{ mol}^{-1}$  (see Table S3, Supporting Information); this agrees with the understanding that methanol is formed, on Cu/CeO<sub>2</sub>, via the RWGS pathway, with CO being a key intermediate [30]. Desorption of CO competes with its further hydrogenation, resulting in low methanol selectivity. For Cu/CeW<sub>0.25</sub>O<sub>x</sub>, the apparent activation energies of methanol formation and CO formation are  $38 \pm 2$  and  $58 \pm 2 \text{ kJ mol}^{-1}$ , respectively (Table S3, Supporting Information). This disparity in activation energy suggests that RWGS is unlikely to be the rate-controlling step for methanol formation on Cu/CeW<sub>0.25</sub>O<sub>x</sub>.

The catalytic mechanism of CO<sub>2</sub> hydrogenation was investigated by in situ DRIFTS, the results of which are shown in Fig. 3. After 30 min of CO<sub>2</sub> hydrogenation at 250 °C, 35 bar, the surface of Cu/CeW<sub>0.25</sub>O<sub>x</sub> showed adsorbates including adsorbed CO (2077 cm<sup>-1</sup>), formate (the peaks at 1601, 1378, 1078 and 2842 cm<sup>-1</sup> correspond to the symmetric vibration of  $\nu(\text{OCO})$ , the asymmetric vibration  $\nu_s(\text{OCO})$ , the stretching vibration of -OCH and the stretching of -CH, respectively), carbonates (1432 cm<sup>-1</sup>), HOCO ( $\sim 1580 \text{ cm}^{-1}$ ) and possibly trace amount of HCO<sub>3</sub> (1622 and 1222 cm<sup>-1</sup>) [64]. The low intensity of the CO peak at 2077 cm<sup>-1</sup> suggests that CO adsorption on Cu is indeed weak [65,66]. After purging the reaction cell with He for 120 min, the adsorption peaks of CO and HCO<sub>3</sub> disappeared owing to their weak adsorption. Then, H<sub>2</sub> was supplied to the purged reaction cell to hydrogenate the remaining adsorbates. From the time-resolved DRIFTS spectra, it can be seen that the intensity of the formate peaks decreased gradually over time, accompanied by the emergence of characteristic peaks corresponding to surface methoxy species at 2924 cm<sup>-1</sup>, 2796 cm<sup>-1</sup> and 1064 cm<sup>-1</sup> [21]. The observation of the methoxy group as a surface-significant species, in conjunction with the increase in methanol yield, suggests that methoxy is a key intermediate for methanol formation, in agreement with the literature [52]. The dynamic spectral changes indicate that methanol is formed via the formate pathway on Cu/CeW<sub>0.25</sub>O<sub>x</sub>.

On Cu/CeO<sub>2</sub>, the same surface adsorbates were observed during

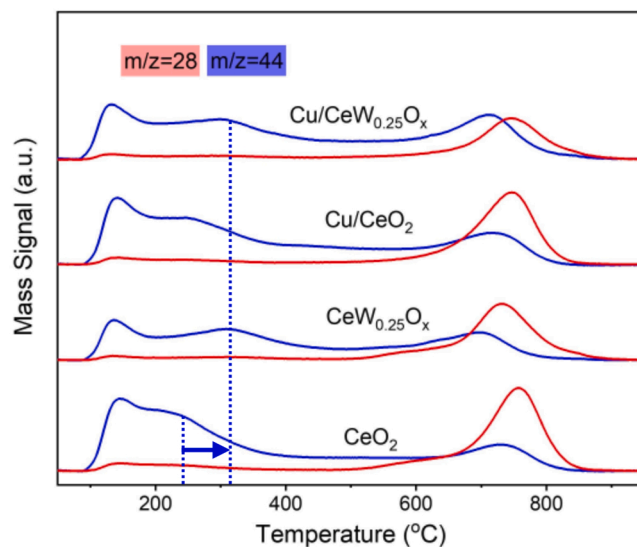


**Fig. 4.** CO<sub>2</sub>-TPD profiles of the CeO<sub>2</sub>-based supports and the Cu loaded catalysts. The vertical blue lines indicate the shift of the CO<sub>2</sub> desorption peak.

steady-state hydrogenation (viz. CO, HCOO and HCO<sub>3</sub>). After purging with He, HCOO is the main surface-significant species, as shown in Fig. S6. However, the formate peaks remained largely unchanged over 300 min of continuous H<sub>2</sub> treatment at 250 °C, 35 bar. Therefore, formate appears to act as a spectator on undoped Cu/CeO<sub>2</sub>, a phenomenon that has been previously reported in the literature [30].

### 3.3. The roles of oxygen vacancies and Ce<sup>3+</sup> sites

On undoped CeO<sub>2</sub>, the presence of Ce<sup>3+</sup> is often associated with the presence of oxygen vacancies, which in turn, is correlated to the redox activity of CeO<sub>2</sub> or the metal/CeO<sub>2</sub> interface. This is not the case for Cu/CeW<sub>0.25</sub>O<sub>x</sub>. In the following, we experimentally verify the lack of correlation between Ce<sup>3+</sup>, oxygen vacancies and redox activity on Cu/CeW<sub>0.25</sub>O<sub>x</sub>. First, CO<sub>2</sub>-TPD was performed to probe the CO<sub>2</sub> affinity and the redox activity of the catalysts, as shown in Fig. 4. Over the

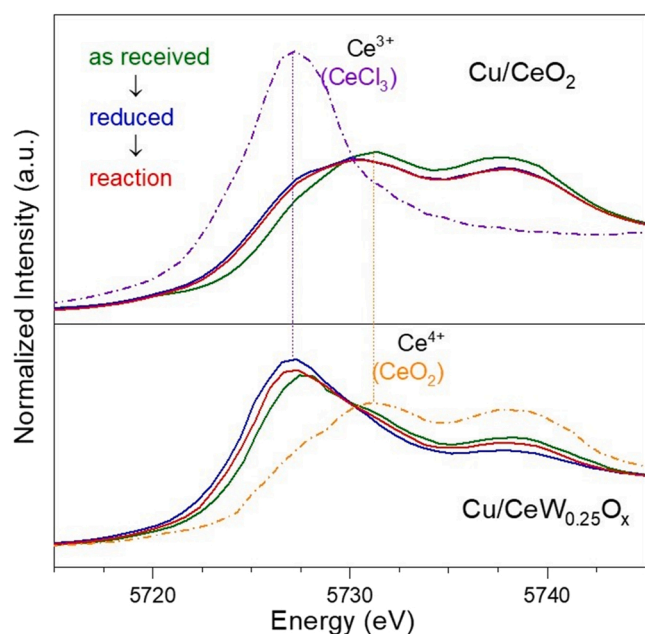


**Fig. 5.** In situ XANES spectra of Ce L<sub>III</sub> edge of the catalysts when freshly calcined (“as received”, green line), after reduction in 10% H<sub>2</sub>/He at 500 °C, 10 bar for 30 min (“reduced”, blue line), and during CO<sub>2</sub> hydrogenation in a 23:69:8 mixture of CO<sub>2</sub>/H<sub>2</sub>/N<sub>2</sub> at 250 °C, 10 bar, after 30 min TOS (“reaction”, red line). The purple and orange dash-dot line refer to Ce<sup>3+</sup> (CeCl<sub>3</sub>) and Ce<sup>4+</sup> (CeO<sub>2</sub>) references, respectively.

unmodified CeO<sub>2</sub> support, a CO<sub>2</sub> desorption peak at 140 °C, with a shoulder at ~240 °C was observed, whereas a second CO<sub>2</sub> desorption peak can be seen ~760 °C. Upon W-doping, the shoulder peak ~240 °C shifted to ~320 °C, suggesting stronger CO<sub>2</sub> adsorption. The high temperature CO<sub>2</sub> desorption peaks ( $m/z = 44$ ) above 700 °C are accompanied by CO desorption peaks ( $m/z = 28$ , after correcting for the  $m/z = 28$  contribution by CO<sub>2</sub> fragmentation). The CO produced is attributed to the dissociative adsorption of CO<sub>2</sub> at an oxygen vacancy site [67]. Therefore, the amount of CO produced is indicative of the amount of redox-active oxygen vacancies (i.e. the oxygen vacancies that could reversibly form and disappear upon reduction and oxidation, respectively) present in the surface-region of the catalyst. To complement, we define the non-redox-active oxygen vacancies to be those originating from the inherent defects of the structures of the metal oxides. Therefore, the amount of non-redox-active oxygen vacancies would remain largely unchanged over varying redox environments. Accordingly, the quantifications of the redox-active oxygen vacancies are shown in Table S4. The fact that Cu/CeW<sub>0.25</sub>O<sub>x</sub> and CeW<sub>0.25</sub>O<sub>x</sub> produced less CO than Cu/CeO<sub>2</sub> and CeO<sub>2</sub> suggests W-doping suppresses the redox activity of CeO<sub>2</sub>, with or without Cu loading. This also agrees well with the O<sub>2</sub>-TPO results, as shown in Fig. S7, i.e. pre-reduced CeO<sub>2</sub> consumes more O<sub>2</sub> (452 μmol/g) and is more redox-active than the pre-reduced CeW<sub>0.25</sub>O<sub>x</sub> (with an oxygen consumption of 283 μmol/g).

The relative concentrations of Ce<sup>3+</sup> and Ce<sup>4+</sup> under pressurised CO<sub>2</sub> hydrogenation conditions were studied by in situ XANES, the results of which are shown in Fig. 5. By performing linear combination fitting (LCF) of the XANES data, the mole fraction of Ce<sup>3+</sup> (balanced by Ce<sup>4+</sup>) in the catalysts can be estimated. The results of the LCF analyses are shown in Table S5 and discussed below. The air calcined CuO/CeO<sub>2</sub> catalyst precursor exhibits a typical Ce-L<sub>III</sub> edge matching that of the reference CeO<sub>2</sub>, showing 0% Ce<sup>3+</sup>. H<sub>2</sub> treatment at 500 °C resulted in the formation of oxygen vacancies and 17% Ce<sup>3+</sup>, as Ce-L<sub>III</sub> edge of the reduced Cu/CeO<sub>2</sub> catalyst moved to a lower energy. Under in situ CO<sub>2</sub> hydrogenation conditions at 250 °C and 10 bar total pressure, the reduced CeO<sub>2</sub> was slightly oxidised by the adsorbed CO<sub>2</sub> to produce CO [39,40], accompanied by the elimination of a small fraction of oxygen vacancies

and a slight decrease in the mole fraction of Ce<sup>3+</sup> from 17% to 15%.

Compared to Cu/CeO<sub>2</sub>, the Ce-L<sub>III</sub> edge of Cu/CeW<sub>0.25</sub>O<sub>x</sub> responds to changes in the gas environment differently. The CuO/CeW<sub>0.25</sub>O<sub>x</sub> catalyst precursor, after calcination in air, already contains 49% Ce<sup>3+</sup>. The Ce<sup>3+</sup> content in air-calcined CuO/CeW<sub>0.25</sub>O<sub>x</sub> corresponds well to the Ce:W ratio of 4:1 and the fact that each W<sup>6+</sup> could reduce two adjacent Ce<sup>4+</sup> to Ce<sup>3+</sup>. H<sub>2</sub> reduction at 500 °C and CO<sub>2</sub> hydrogenation reaction at 250 °C further increased the mole fraction of Ce<sup>3+</sup> to 69% and 59%, respectively, whilst creating additional oxygen vacancies in the catalysts. Here, the changes in the amount of Ce<sup>3+</sup> under varying gas environments characterise the redox activity of the catalyst, subject to practical limitations: (i) XANES is not a surface-sensitive technique and (ii) the measurements may not capture all the transient redox processes taking place [68]. Based on the trends observed, the bulk redox activities of Cu/CeO<sub>2</sub> and Cu/CeW<sub>0.25</sub>O<sub>x</sub> appears similar.

The in situ EXAFS data of the Cu-K edge of both catalysts are carefully fitted by a single Cu-Cu shell (see Fig. S8, Supporting Information). The fitting results suggest average Cu-Cu first shell coordination numbers of 9.1 and 9.5 for Cu/CeO<sub>2</sub> and Cu/CeW<sub>0.25</sub>O<sub>x</sub>, respectively (Table S6, Supporting Information), with mean Cu particle sizes of 3.2 nm and 3.5 nm, respectively, assuming spherical particle shapes [69]. The particle sizes estimated by EXAFS are close to the size estimates by HRTEM and N<sub>2</sub>O chemisorption analyses (i.e. ~4 nm).

The chemical states of the surface regions of the catalysts were probed in situ by NAP-XPS. The signal-to-noise ratio in the C 1s region of the measured XPS spectra was too low to perform any meaningful interpretation, whereas the Cu 2p, Ce 3d, O 1s and W 4f regions, shown in Fig. 6, were analysed in detail. The Cu 2p spectra of both Cu/CeO<sub>2</sub> and Cu/CeW<sub>0.25</sub>O<sub>x</sub>, when (i) freshly reduced, (ii) oxidised by CO<sub>2</sub> at RT and (iii) under CO<sub>2</sub> hydrogenation conditions at 250 °C (Fig. 6a and b), show the predominance of Cu<sup>0</sup> species in the surface regions of the catalysts under CO<sub>2</sub> hydrogenation conditions at 1.2 mbar, 250 °C. Given the similarity of the positions of the Cu<sup>0</sup> peaks (933 eV) of the two catalyst samples, it is plausible that W-doping does not have a notable influence on the chemical state of the Cu<sup>0</sup> sites; this agrees with the similar Cu Auger spectra of the two catalysts (Fig. S4). After O<sub>2</sub> treatment, the surface regions (and quite possibly the bulk) of the Cu particles were oxidised to Cu<sup>2+</sup> for both Cu/CeO<sub>2</sub> and Cu/CeW<sub>0.25</sub>O<sub>x</sub>, as shown in Fig. 6c. Likewise, the similar Cu 2p peaks of the oxidised Cu/CeO<sub>2</sub> and Cu/CeW<sub>0.25</sub>O<sub>x</sub> are in line with the complementary experimental observations that W-doped does not have a significant effect on the chemical state of Cu.

The Ce 3d XPS spectra, plotted in Fig. 6d and e, show trends agreeing well with the in situ XANES results, i.e., the surface region of the W-doped catalyst contains significantly more Ce<sup>3+</sup>, with only a small fraction of Ce<sup>3+</sup> oxidisable by CO<sub>2</sub> (viz. in CO<sub>2</sub> at RT and CO<sub>2</sub> + H<sub>2</sub> at 250 °C). In all NAP-XPS measurements, the surface region of Cu/CeW<sub>0.25</sub>O<sub>x</sub> consistently contained more Ce<sup>3+</sup> than that of Cu/CeO<sub>2</sub>, signifying the reduction of Ce<sup>4+</sup> to Ce<sup>3+</sup> and the stabilisation of the Ce<sup>3+</sup> by W-doping. On the other hand, the surface region of the reduced Cu/CeO<sub>2</sub> appears more redox active (the Ce<sup>3+</sup> content changes from 28.2% to 15.6% by CO<sub>2</sub> oxidation) than that of Cu/CeW<sub>0.25</sub>O<sub>x</sub> (the Ce<sup>3+</sup> content changes from 40.8% to 38.3%). Therefore, although Cu/CeW<sub>0.25</sub>O<sub>x</sub> has more Ce<sup>3+</sup> in its surface region than Cu/CeO<sub>2</sub>, the majority of the Ce<sup>3+</sup> species are not redox-active. It is plausible that these non-redox-active Ce<sup>3+</sup> are responsible for the significantly enhanced methanol synthesis activity of Cu/CeW<sub>0.25</sub>O<sub>x</sub>.

The XPS in the O 2p region also correlates well with the Ce 3d spectra. For Cu/CeO<sub>2</sub> (Fig. 6f), the peak at 529.3 eV (denoted as O<sub>β</sub>) can be assigned to O<sup>2-</sup> located near the Ce<sup>4+</sup> ions [70], whereas the peak at 531.5 eV (denoted as O<sub>α</sub>) is assigned to the carbonate-like and hydroxy adsorbates on the oxygen vacancy sites [71]. For Cu/CeW<sub>0.25</sub>O<sub>x</sub> (Fig. 6g), the peak at 530.5 eV (O<sub>β</sub>) is assigned to O<sup>2-</sup> located near the Ce<sup>3+</sup> ions [70,72], accompanied by the small peak at 532.6 eV (O<sub>α</sub>), which is characteristic of the adsorbate-related contribution associated with oxygen vacancies. Therefore, the apparent shifts in the binding

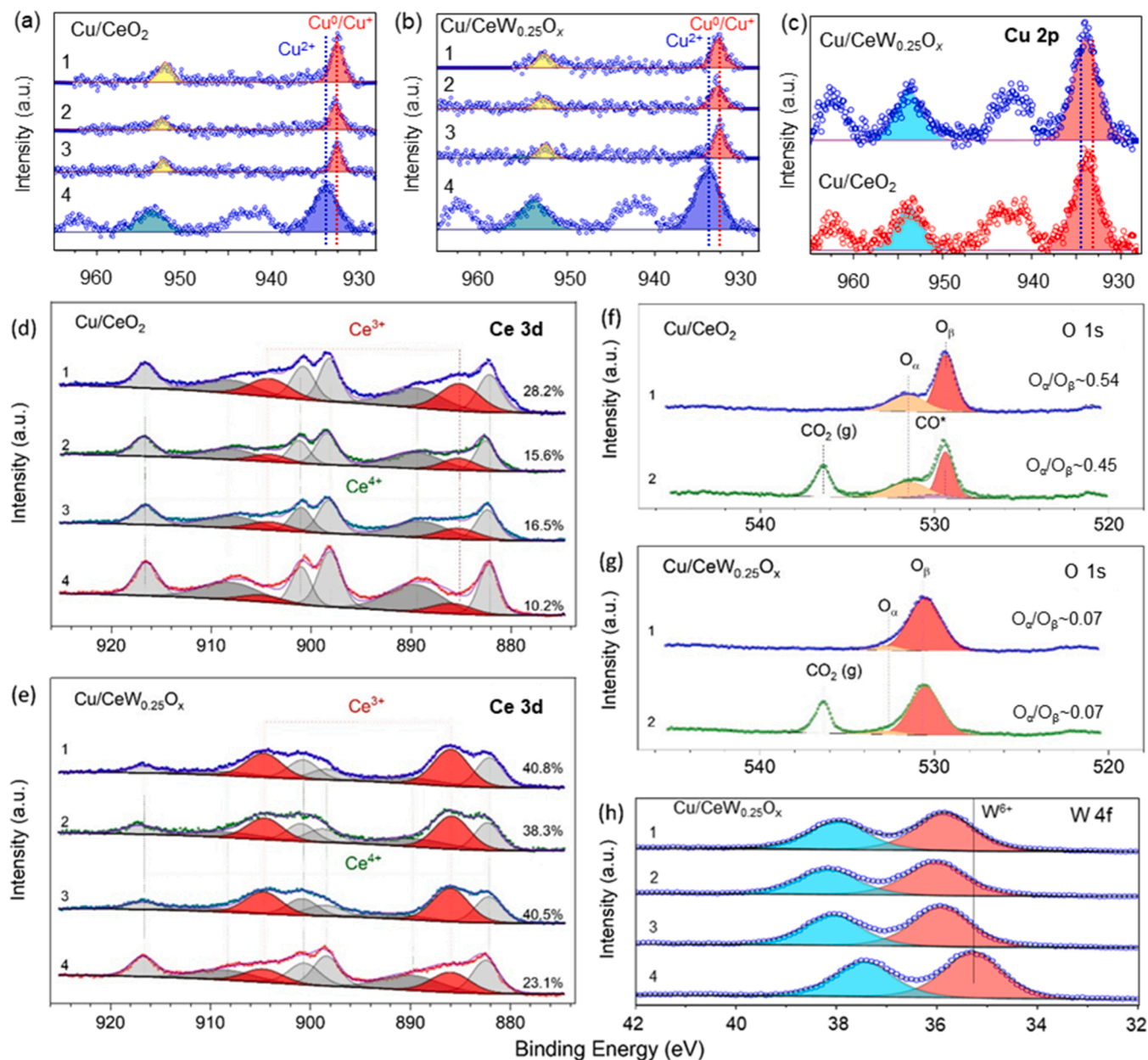
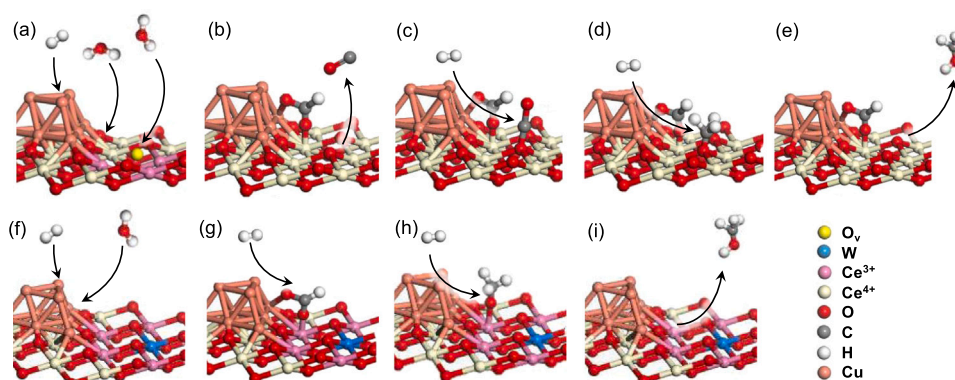


**Fig. 6.** High-resolution XPS spectra obtained during the NAP-XPS experiments. (a) and (b) show the Cu 2p region. (c) shows the close inspection of the Cu 2p spectra after oxidation. (d) and (e) show the Ce 3d region, with the fractions of  $\text{Ce}^{3+}$  in the surface regions of the catalysts labelled on the right of each spectrum. (f) and (g) show the O 1s region. (h) shows the W 4f region; the dashed vertical line denotes the reference binding energy of  $\text{WO}_3$ . XPS measurements were taken when each sample was subjected to the following environments, in chronological order, 1) “reduced”: 0.4 mbar  $\text{H}_2$  at 500 °C, 2) “ $\text{CO}_2$  RT”: 0.5 mbar  $\text{CO}_2$  at RT, 3) “ $\text{CO}_2$ + $\text{H}_2$ @ 250°”: 0.3 mbar  $\text{CO}_2$  and 0.9 mbar  $\text{H}_2$  at 250 °C and 4) “oxidised”: 0.4 mbar  $\text{O}_2$  at 500 °C.

energies of the O 1s XPS upon W-doping can be explained by the change from the  $\text{Ce}^{4+}$ -rich surface of the  $\text{CeO}_2$  support to one that is rich in  $\text{Ce}^{3+}$ . Additionally, the ratio of  $\text{O}_\alpha/\text{O}_\beta$  is indicative of the activity of the oxygen vacancy sites, which could adsorptively activate  $\text{CO}_2$  and  $\text{H}_2\text{O}$ . Upon the introduction of  $\text{CO}_2$  at RT, the  $\text{O}_\alpha/\text{O}_\beta$  ratio increases from 0.54 to 0.82 on  $\text{Cu/CeO}_2$ , accompanied by the emergence of a peak at 536.3 eV, which corresponds to gaseous  $\text{CO}_2$  molecules (Fig. 6d). In contrast, the  $\text{O}_\alpha/\text{O}_\beta$  ratio on the reduced  $\text{Cu/CeW}_{0.25}\text{O}_x$  hardly changes ( $\sim 0.07$ ) upon exposure to  $\text{CO}_2$ , suggesting that the oxygen vacancies on  $\text{Cu/CeW}_{0.25}\text{O}_x$  have rather lower activity; this is in good agreement with its low CO selectivity observed during  $\text{CO}_2$  hydrogenation experiment (Fig. 1) and the low redox activity observed by  $\text{CO}_2$ -TPD (Fig. 4) and NAP-XPS of the Ce 3d region (Fig. 6e). Fig. 6h plots the W 4f XPS of the  $\text{Cu/CeW}_{0.25}\text{O}_x$  catalyst at various stages of the NAP-XPS experiment. With the

exception of the fully oxidised  $\text{Cu/CeW}_{0.25}\text{O}_x$  (after exposure to  $\text{O}_2$  at 500 °C), the catalyst under otherwise reduced or partially reduced states exhibits W 4f XPS peaks that are shifted to higher binding energies relative to the  $\text{WO}_3$  reference. This observation is in agreement with the theoretical study by Hu and Metiu, who concluded that the W dopant in  $\text{CeO}_2$  would donate electrons to neighbouring  $\text{Ce}^{4+}$  species, forming  $\text{Ce}^{3+}$  sites [42]. The charge transfer from  $\text{W}^{6+}$  to  $\text{Ce}^{3+}$  also corroborated by the NAP-XPS data of the Ce 3d region (Fig. 6d). In addition, the effect of W dopant on the charge transfer mechanism is supported by  $\text{H}_2$ -TPR (Fig. 1e), which portrays a negative shift in  $\text{H}_2$  reduction temperature of  $\text{CeW}_{0.25}\text{O}_x$  after air calcination, indicating higher reducibility of  $\text{CeW}_{0.25}\text{O}_x$  as compared to  $\text{CeO}_2$ .

Based on the experimental results discussed above, the catalytic consequences of W-doping are summarised in the following: (i) reducing



**Scheme 1.** Proposed reaction mechanisms for CO<sub>2</sub> hydrogenation on (a–e) unmodified Cu/CeO<sub>2</sub> and (f–i) Cu/CeW<sub>0.25</sub>O<sub>x</sub>. The key steps on Cu/CeO<sub>2</sub> include: (a) activation of H<sub>2</sub> on Cu with hydrogen spillover across the Cu/CeO<sub>2</sub> interface, activation of CO<sub>2</sub> at the Cu/CeO<sub>2</sub> interface, and activation of CO<sub>2</sub> on an oxygen vacancy (O<sub>v</sub>) of CeO<sub>2</sub>; (b) desorption of CO produced by the dissociative adsorption of CO<sub>2</sub> at an oxygen vacancy, leaving behind formate spectators; (c) successive hydrogenation of adsorbed \*CO species to form methoxy; (d) hydrogenation of surface methoxy species forming methanol; (e) desorption of methanol, leaving behind surface formate spectators. The key steps on Cu/CeW<sub>0.25</sub>O<sub>x</sub> include: (f) activation of H<sub>2</sub> on Cu with hydrogen spillover across the Cu/CeO<sub>2</sub> interface and activation of CO<sub>2</sub> at

the Cu/CeW<sub>0.25</sub>O<sub>x</sub> interface; (g) successive hydrogenation of formate species at the Cu/CeW<sub>0.25</sub>O<sub>x</sub> interface to form surface methoxy species; (h) hydrogenation of surface methoxy species to form methanol; (i) desorption of methanol.

Ce<sup>4+</sup> to Ce<sup>3+</sup> and stabilising Ce<sup>3+</sup> both in the surface region and the bulk of the Cu/CeW<sub>0.25</sub>O<sub>x</sub> catalyst, (ii) suppressing the redox activity of the Cu/CeW<sub>0.25</sub>O<sub>x</sub> catalyst, (iii) promoting the formate pathway for CO<sub>2</sub> hydrogenation to methanol, and (iv) improving both CO<sub>2</sub> activation and selectivity towards methanol. Accordingly, the structural-functional relationship of the W-doped Cu/CeW<sub>0.25</sub>O<sub>x</sub> catalyst, is depicted in Scheme 1 and elaborated below.

During CO<sub>2</sub> hydrogenation on unmodified Cu/CeO<sub>2</sub>, the Cu nanoparticles facilitate hydrogen activation (including H<sub>2</sub> spill-over, Scheme 1a), whilst the redox-active oxygen vacancies formed on CeO<sub>2</sub> promote the dissociative activation of CO<sub>2</sub> to CO, i.e., RWGS via the Mars-van Krevelen (MvK) mechanism (Scheme 1b). Concomitantly, a fraction of the catalyst surface (possibly on the Cu and at the Cu/CeO<sub>2</sub> interfaces [30,73–75]) is covered by formate spectators (Scheme 1a). As such, the formation of CO, with an apparent activation energy of 55 kJ mol<sup>−1</sup>, is the rate limiting step for methanol formation on unmodified Cu/CeO<sub>2</sub>. While the hydrogen of adsorbed CO produces methanol (Scheme 1c–e) The weak adsorption of CO on Cu results in low methanol selectivity and productivity.

For Cu/CeW<sub>0.25</sub>O<sub>x</sub>, the W dopants donate electrons to the neighbouring Ce<sup>4+</sup>, generating and stabilising substantial amount of non-redox-active Ce<sup>3+</sup> (Scheme 1f). The lack of reducibility of Ce<sup>3+</sup> and W<sup>6+</sup>, as shown by the NAP-XPS spectra in Fig. 6e and h, hinders the ability of Cu/CeW<sub>0.25</sub>O<sub>x</sub> to lose lattice oxygen and create redox-active oxygen vacancies under CO<sub>2</sub> hydrogenation conditions, thus suppressing its redox activity. Consequently, RWGS and CO selectivity are effectively suppressed. Furthermore, the presence of the W-stabilised, non-redox-active Ce<sup>3+</sup> species in the Cu/CeW<sub>0.25</sub>O<sub>x</sub> catalyst promote the hydrogenation of the surface formate species (Scheme 1g), activating the formate pathway to become the dominant reaction pathway (Scheme 1h,i) with a significantly reduced apparent activation energy of 38 kJ mol<sup>−1</sup> and a 10-fold increase in methanol STY.

The proposed structural-functional relationship is in line with the study by Senanayake et al. [76], who correlated the surface concentration of stable Ce<sup>3+</sup> to the apparent rate of methanol formation. The improved CO<sub>2</sub> conversion with increasing Ce<sup>3+</sup> is also corroborated by previous studies reporting that the Ce<sup>3+</sup> sites on CeO<sub>2</sub> are responsible for the adsorptive activation of CO<sub>2</sub> [77–79]. However, the mechanistic function of the W-stabilised Ce<sup>3+</sup> during the Cu-catalysed CO<sub>2</sub> hydrogenation is not fully understood and merits in-depth investigations in future studies, preferably with the help of theoretical tools such as density-functional theory calculations.

#### 4. Conclusions

We prepared a Cu/CeW<sub>0.25</sub>O<sub>x</sub> catalyst for CO<sub>2</sub> hydrogenation to

produce methanol. W-doping increases and stabilises the concentration of non-redox-active Ce<sup>3+</sup> on Cu/CeW<sub>0.25</sub>O<sub>x</sub>, resulting in significantly enhanced methanol productivity and selectivity. The W-induced reduction of Ce<sup>4+</sup> also uncouples the catalytic roles of oxygen vacancies and that of the Ce<sup>3+</sup> species. On unmodified Cu/CeO<sub>2</sub>, CO<sub>2</sub> is activated either (i) dissociatively at a redox-active oxygen vacancy on CeO<sub>2</sub>, forming a weakly adsorbing \*CO or (ii) forming a stable formate spectator. Subsequently, CO<sub>2</sub> is hydrogenated via the RWGS pathway with inherently low methanol selectivity. In comparison, W-doping resulted in a considerably reduced CeO<sub>2</sub> surface having low redox activity and suppressed CO selectivity. This is achieved by W donating electrons to neighbouring Ce<sup>4+</sup>, reducing them to Ce<sup>3+</sup> without generating additional oxygen vacancies. The abundant non-redox-active Ce<sup>3+</sup> species on Cu/CeW<sub>0.25</sub>O<sub>x</sub> promote the hydrogenation of formate to produce methanol at a rate that is 10 times faster than undoped Cu/CeO<sub>2</sub>. Beyond CO<sub>2</sub> hydrogenation, high-valency cation doping may be further exploited as a means to tune the catalytic activity of CeO<sub>2</sub> for reactions where high redox activity is undesired.

#### Funding sources

National Research Foundation of Singapore: Campus for Research Excellence and Technological Enterprise (CREATE) programme.

Ministry of Education, Singapore: Academic Research Funding Tier 1: RT03/19.

#### CRediT authorship contribution statement

**Yong Yan:** Conceptualization, Methodology, Formal analysis, Investigation, Writing – original draft, Visualization. **Roong Jien Wong:** Methodology, Formal analysis, Investigation, Visualization, Writing – review & editing. **Zhirui Ma:** Formal analysis, Investigation. **Felix Donat:** Formal analysis, Investigation, Writing – review & editing. **Shibo Xi:** Formal analysis, Investigation. **Syed Saqline:** Investigation. **Qianwenhao Fan:** Investigation. **Yonghua Du:** Investigation. **Armando Borgna:** Resources, Supervision. **Qian He:** Investigation. **Christoph R. Müller:** Resources, Supervision, Writing – review & editing. **Wei Chen:** Resources, Supervision. **Alexei A. Lapkin:** Resources, Writing – review & editing, Supervision. **Wen Liu:** Resources, Writing – review & editing, Supervision.

#### Declaration of Competing Interest

The authors declare that they have no known competing financial interests or personal relationships that could have appeared to influence the work reported in this paper.

## Acknowledgement

This research is funded by the National Research Foundation (NRF), Prime Minister's Office, Singapore under its Campus for Research Excellence and Technological Enterprise (CREATE) programme and Ministry of Education, Singapore under its AcRF Tier 1 (RT03/19). The authors would also like to thank Prof. Kongzhai Li from Kunming University of Science and Technology for the helpful discussions.

## Author contributions

The manuscript was written through contributions of all authors. All authors have given approval to the final version of the manuscript.

## Supporting information

The following files are available free of charge. Supporting information.pdf (PDF).

## Appendix A. Supporting information

Supplementary data associated with this article can be found in the online version at [doi:10.1016/j.apcatb.2022.121098](https://doi.org/10.1016/j.apcatb.2022.121098).

## References

- [1] R.M. Cuéllar-Franca, A. Azapagic, Carbon Capture, storage and utilisation technologies: a critical analysis and comparison of their life cycle environmental impacts, *J. CO<sub>2</sub> Util.* 9 (2015) 82–102, <https://doi.org/10.1016/j.jcou.2014.12.001>.
- [2] M. Bui, C.S. Adjiman, A. Bardow, E.J. Anthony, A. Boston, S. Brown, P.S. Fennell, S. Fuss, A. Galindo, L.A. Hackett, J.P. Hallett, H.J. Herzog, G. Jackson, J. Kemper, S. Krevor, G.C. Maitland, M. Matuszewski, I.S. Metcalfe, C. Petit, G. Puxty, J. Reimer, D.M. Reiner, E.S. Rubin, S.A. Scott, N. Shah, B. Smit, J.P.M. Trusler, P. Webley, J. Wilcox, N.M. Dowell, Carbon capture and storage (CCS): the way forward, *Energy Environ. Sci.* 11 (5) (2018) 1062–1176, <https://doi.org/10.1039/C7EE02342A>.
- [3] A. Käthelhö, R. Meys, S. Deutz, S. Suh, A. Bardow, Climate change mitigation potential of carbon capture and utilization in the chemical industry, *PNAS* 116 (23) (2019) 11187–11194, <https://doi.org/10.1073/pnas.1821029116>.
- [4] J. Rissman, C. Bataille, E. Masanet, N. Aden, W.R. Morrow, N. Zhou, N. Elliott, R. Dell, N. Heeren, B. Hucklestein, J. Cresko, S.A. Miller, J. Roy, P. Fennell, B. Cremmins, T. Koch Blank, D. Hone, E.D.; Williams, S.; de la Rue du Can, B.; Sisson, M.; Williams, J.; Katzenberger, D.; Burtraw, G.; Sethi, H.; Ping, D.; Danielson, H.; Lu, T.; Lorber, J.; Dinkel, J. Helseth, Technologies and policies to decarbonize global industry: review and assessment of mitigation Drivers through 2070, *Appl. Energy* 266 (2020), 114848, <https://doi.org/10.1016/j.apenergy.2020.114848>.
- [5] L. Tao, T.S. Choksi, W. Liu, J. Pérez-Ramírez, Synthesizing high-volume chemicals from CO<sub>2</sub> without direct H<sub>2</sub> input, *ChemSusChem* n/a (n/a), <https://doi.org/10.1002/cssc.202001604>.
- [6] M.D. Burkart, N. Hazari, C.L. Tway, E.L. Zeitler, Opportunities and challenges for catalysis in carbon dioxide utilization, *ACS Catal.* 9 (9) (2019) 7937–7956, <https://doi.org/10.1021/acscatal.9b02113>.
- [7] C. Jia, J. Gao, Y. Dai, J. Zhang, Y. Yang, The thermodynamics analysis and experimental validation for complicated systems in CO<sub>2</sub> hydrogenation process, *J. Energy Chem.* 25 (6) (2016) 1027–1037, <https://doi.org/10.1016/j.jechem.2016.10.003>.
- [8] M. Yang, D. Fan, Y. Wei, P. Tian, Z. Liu, Recent progress in methanol-to-olefins (MTO) catalysts, *Adv. Mater.* 31 (50) (2019), 1902181, <https://doi.org/10.1002/adma.201902181>.
- [9] J. Ashok L. Falbo S. Das N. Dewangan C.G. Visconti S. Kawi, Catalytic CO<sub>2</sub> conversion to added-value energy rich C1 products. an economy based on carbon dioxide and water, 2019, 155–210. doi: 10.1007/978-3-030-15868-2.5.
- [10] A.A. Tountas, X. Peng, A.V. Tavasoli, P.N. Duchesne, T.L. Dingle, Y. Dong, L. Hurtado, A. Mohan, W. Sun, U. Ulmer, L. Wang, T.E. Wood, C.T. Maravelias, M. M. Sain, G.A. Ozin, Towards solar methanol: past, present, and future, *Adv. Sci.* 6 (8) (2019), 1801903, <https://doi.org/10.1002/adv.201801903>.
- [11] A. González-Garay, M.S. Frei, A. Al-Qahtani, C. Mondelli, G. Guillén-Gosálbez, J. Pérez-Ramírez, Plant-to-planet analysis of CO<sub>2</sub>-based methanol processes, *Energy Environ. Sci.* 12 (12) (2019) 3425–3436, <https://doi.org/10.1039/C9EE01673B>.
- [12] B.M. Tackett, E. Gomez, J.G. Chen, Net reduction of CO<sub>2</sub> via its thermocatalytic and electrocatalytic transformation reactions in standard and hybrid processes, *Nat. Catal.* 2 (5) (2019) 381–386, <https://doi.org/10.1038/s41929-019-0266-y>.
- [13] J. Sehested, Industrial and scientific directions of methanol catalyst development, *J. Catal.* 371 (2019) 368–375, <https://doi.org/10.1016/j.jcat.2019.02.002>.
- [14] G.A. Olah, Towards oil independence through renewable methanol chemistry, *Angew. Chem. Int. Ed.* 52 (1) (2013) 104–107, <https://doi.org/10.1002/anie.201204995>.
- [15] B. Liang, J. Ma, X. Su, C. Yang, H. Duan, H. Zhou, S. Deng, L. Li, Y. Huang, Investigation on deactivation of Cu/ZnO/Al<sub>2</sub>O<sub>3</sub> catalyst for CO<sub>2</sub> hydrogenation to methanol, *Ind. Eng. Chem. Res.* 58 (21) (2019) 9030–9037, <https://doi.org/10.1021/acs.iecr.9b01546>.
- [16] J. Zhong, X. Yang, Z. Wu, B. Liang, Y. Huang, T. Zhang, State of the art and perspectives in heterogeneous catalysis of CO<sub>2</sub> hydrogenation to methanol, *Chem. Soc. Rev.* 49 (5) (2020) 1385–1413, <https://doi.org/10.1039/C9CS00614A>.
- [17] T. Fujitani, M. Saito, Y. Kanai, T. Watanabe, J. Nakamura, T. Uchijima, Development of an active Ga<sub>2</sub>O<sub>3</sub> supported palladium catalyst for the synthesis of methanol from carbon dioxide and hydrogen, *Appl. Catal. A: Gen.* 125 (2) (1995) L199–L202, [https://doi.org/10.1016/0926-860X\(95\)00049-6](https://doi.org/10.1016/0926-860X(95)00049-6).
- [18] F. Arena, G. Mezzatesta, G. Zafarana, G. Trunfio, F. Frusteri, L. Spadaro, Effects of oxide carriers on surface functionality and process performance of the Cu–ZnO system in the synthesis of methanol via CO<sub>2</sub> hydrogenation, *J. Catal.* 300 (2013) 141–151, <https://doi.org/10.1016/j.jcat.2012.12.019>.
- [19] N. Rui, Z. Wang, K. Sun, J. Ye, Q. Ge, C. Liu, CO<sub>2</sub> hydrogenation to methanol over Pd/In<sub>2</sub>O<sub>3</sub>: effects of Pd and oxygen vacancy, *Appl. Catal. B: Environ.* 218 (2017) 488–497, <https://doi.org/10.1016/j.apcatb.2017.06.069>.
- [20] S. Bai, Q. Shao, Y. Feng, L. Bu, X. Huang, Highly efficient carbon dioxide hydrogenation to methanol catalyzed by zigzag platinum–cobalt nanowires, *Small* 13 (22) (2017), 1604311, <https://doi.org/10.1002/sml.201604311>.
- [21] J. Wang, G. Li, Z. Li, C. Tang, Z. Feng, H. An, H. Liu, T. Liu, C. Li, A highly selective and stable ZnO–ZrO<sub>2</sub> solid solution catalyst for CO<sub>2</sub> hydrogenation to methanol, *Sci. Adv.* 3 (10) (2017), e1701290, <https://doi.org/10.1126/sciadv.1701290>.
- [22] A. Tsoukalou, P.M. Abdala, D. Stoian, X. Huang, M.-G. Willinger, A. Fedorov, C. R. Müller, Structural evolution and dynamics of an In<sub>2</sub>O<sub>3</sub> catalyst for CO<sub>2</sub> hydrogenation to methanol: an operando XAS-XRD and in situ TEM study, *J. Am. Chem. Soc.* 141 (34) (2019) 13497–13505, <https://doi.org/10.1021/jacs.9b04873>.
- [23] M.S. Frei, C. Mondelli, R. García-Muelas, K.S. Kley, B. Puértolas, N. López, O. V. Safonova, J.A. Stewart, D. Curulla Ferré, J. Pérez-Ramírez, Atomic-scale engineering of indium oxide promotion by palladium for methanol production via CO<sub>2</sub> hydrogenation, *Nat. Commun.* 10 (1) (2019) 1–11, <https://doi.org/10.1038/s41467-019-11349-9>.
- [24] Y. Li, S.H. Chan, Q. Sun, Heterogeneous catalytic conversion of CO<sub>2</sub>: a comprehensive theoretical review, *Nanoscale* 7 (19) (2015) 8663–8683, <https://doi.org/10.1039/C5NR00092K>.
- [25] S. Kattel, P. Liu, J.G. Chen, Tuning selectivity of CO<sub>2</sub> hydrogenation reactions at the metal/oxide interface, *J. Am. Chem. Soc.* 139 (29) (2017) 9739–9754, <https://doi.org/10.1021/jacs.7b05362>.
- [26] X. Nie, W. Li, X. Jiang, X. Guo, C. Song, Chapter two – Recent advances in catalytic CO<sub>2</sub> hydrogenation to alcohols and hydrocarbons, in: C. Song (Ed.), *Advances in Catalysis*, Vol. 65, Academic Press, 2019, pp. 121–233, <https://doi.org/10.1016/b.scat.2019.10.002>.
- [27] X. Jiang, X. Nie, X. Guo, C. Song, J.G. Chen, Recent advances in carbon dioxide hydrogenation to methanol via heterogeneous catalysis, *Chem. Rev.* 120 (2020) 7984–8034, <https://doi.org/10.1021/acs.chemrev.9b00723>.
- [28] M. Bowker, Methanol synthesis from CO<sub>2</sub> hydrogenation, *ChemCatChem* 11 (17) (2019) 4238–4246, <https://doi.org/10.1002/cctc.201900401>.
- [29] S. Dang, H. Yang, P. Gao, H. Wang, X. Li, W. Wei, Y. Sun, A review of research progress on heterogeneous catalysts for methanol synthesis from carbon dioxide hydrogenation, *Catal. Today* 330 (2019) 61–75, <https://doi.org/10.1016/j.cattod.2018.04.021>.
- [30] J. Graciani, K. Mudiyanse, F. Xu, A.E. Baber, J. Evans, S.D. Senanayake, D. J. Stacchiola, P. Liu, J. Hrbek, J.F. Sanz, J.A. Rodriguez, Highly active copper-ceria and copper-ceria-titania catalysts for methanol synthesis from CO<sub>2</sub>, *Science* 345 (6196) (2014) 546–550, <https://doi.org/10.1126/science.1253057>.
- [31] A. Rodriguez, J.; C. Grinter, D.; Liu, Z.; M. Palomino, R.; D. Senanayake, S., Ceria-based model catalysts: fundamental studies on the importance of the metal–ceria interface in CO oxidation, the water–gas shift, CO<sub>2</sub> hydrogenation, and methane and alcohol reforming, *Chem. Soc. Rev.* 46 (7) (2017) 1824–1841, <https://doi.org/10.1039/C6CS00863A>.
- [32] G. Vilé, S. Colussi, F. Krumeich, A. Trovarelli, J. Pérez-Ramírez, Opposite face sensitivity of CeO<sub>2</sub> in hydrogenation and oxidation catalysis, *Angew. Chem. Int. Ed.* 53 (45) (2014) 12069–12072, <https://doi.org/10.1002/anie.201406637>.
- [33] A. Trovarelli, J. Llorca, Ceria catalysts at nanoscale: how do crystal shapes shape catalysis? *ACS Catal.* 7 (7) (2017) 4716–4735, <https://doi.org/10.1021/acscatal.7b01246>.
- [34] T. Montini, M. Melchionna, M. Monai, P. Fornasiero, Fundamentals and catalytic applications of CeO<sub>2</sub>-based materials, *Chem. Rev.* 116 (10) (2016) 5987–6041, <https://doi.org/10.1021/acs.chemrev.5b00603>.
- [35] R. Schmitt, A. Nanning, O. Kravynis, R. Korobko, I. Frenkel, A. Lubomirsky, I.; M. Haile, S.; M. Rupp, J. L., A review of defect structure and chemistry in ceria and its solid solutions, *Chem. Soc. Rev.* 49 (2) (2020) 554–592, <https://doi.org/10.1039/C9CS00588A>.
- [36] B. Xu, H. Yang, Q. Zhang, S. Yuan, A. Xie, M. Zhang, T. Ohno, Design and synthesis of Sm, Y, La and Nd-doped CeO<sub>2</sub> with a broom-like hierarchical structure: a photocatalyst with enhanced oxidation performance, *ChemCatChem* 12 (9) (2020) 2638–2646, <https://doi.org/10.1002/cctc.201902309>.
- [37] S. Jiang, R. Zhang, H. Liu, Y. Rao, Y. Yu, S. Chen, Q. Yue, Y. Zhang, Y. Kang, Promoting formation of oxygen vacancies in two-dimensional cobalt-doped ceria nanosheets for efficient hydrogen evolution, *J. Am. Chem. Soc.* 142 (14) (2020) 6461–6466, <https://doi.org/10.1021/jacs.9b13915>.

- [38] Z. Zhang, Y. Wang, J. Lu, J. Zhang, M. Li, X. Liu, F. Wang, Pr-doped CeO<sub>2</sub> catalyst in the prins condensation–hydrolysis reaction: are all of the defect sites catalytically active? *ACS Catal.* 8 (4) (2018) 2635–2644, <https://doi.org/10.1021/acscatal.7b04500>.
- [39] N. Kumari, M.A. Haider, M. Agarwal, N. Sinha, S. Basu, Role of reduced CeO<sub>2</sub>(110) surface for CO<sub>2</sub> reduction to CO and methanol, *J. Phys. Chem. C* 120 (30) (2016) 16626–16635, <https://doi.org/10.1021/acs.jpcc.6b02860>.
- [40] C. Guo, S. Wei, S. Zhou, T. Zhang, Z. Wang, S.-P. Ng, X. Lu, C.-M.L. Wu, W. Guo, Initial reduction of CO<sub>2</sub> on Pd-, Ru-, and Cu-doped CeO<sub>2</sub>(111) surfaces: effects of surface modification on catalytic activity and selectivity, *ACS Appl. Mater. Interfaces* 9 (31) (2017) 26107–26117, <https://doi.org/10.1021/acsami.7b07945>.
- [41] K. Chang, T. Wang, J.G. Chen, Hydrogenation of CO<sub>2</sub> to methanol over CuCeTiOx catalysts, *Appl. Catal. B: Environ.* 206 (2017) 704–711, <https://doi.org/10.1016/j.apcatb.2017.01.076>.
- [42] Z. Hu, H. Metiu, Effect of dopants on the energy of oxygen-vacancy formation at the surface of ceria: local or global? *J. Phys. Chem. C* 115 (36) (2011) 17898–17909, <https://doi.org/10.1021/jp205432r>.
- [43] K. Chang, H. Zhang, M. Cheng, Q. Lu, Application of ceria in CO<sub>2</sub> conversion catalysis, *ACS Catal.* (2019) 613–631, <https://doi.org/10.1021/acscatal.9b03935>.
- [44] J. Guo, H. Lou, L. Mo, X. Zheng, The reactivity of surface active carbonaceous species with CO<sub>2</sub> and its role on hydrocarbon conversion reactions, *J. Mol. Catal. A: Chem.* 316 (1) (2010) 1–7, <https://doi.org/10.1016/j.molcata.2009.09.023>.
- [45] F. Arena, G. Mezzatesta, G. Zafarana, G. Trunfio, F. Frusteri, L. Spadaro, How oxide carriers control the catalytic functionality of the Cu–ZnO system in the hydrogenation of CO<sub>2</sub> to methanol, *Catal. Today* 210 (2013) 39–46, <https://doi.org/10.1016/j.cattod.2013.02.016>.
- [46] L. Angelo, M. Girleanu, O. Ersen, C. Serra, K. Parkhomenko, A.-C. Roger, Catalyst synthesis by continuous coprecipitation under micro-fluidic conditions: application to the preparation of catalysts for methanol synthesis from CO<sub>2</sub>/H<sub>2</sub>, *Catal. Today* 270 (2016) 59–67, <https://doi.org/10.1016/j.cattod.2015.09.028>.
- [47] Q. Tan, Z. Shi, D. Wu, CO<sub>2</sub> hydrogenation to methanol over a highly active Cu–Ni/CeO<sub>2</sub>-nanotube catalyst, *Ind. Eng. Chem. Res.* 57 (31) (2018) 10148–10158, <https://doi.org/10.1021/acs.iecr.8b01246>.
- [48] M. Mureddu, F. Ferrara, A. Pettinau, Highly efficient CuO/ZnO/ZrO<sub>2</sub>@SBA-15 nanocatalysts for methanol synthesis from the catalytic hydrogenation of CO<sub>2</sub>, *Appl. Catal. B: Environ.* 258 (2019), 117941, <https://doi.org/10.1016/j.apcatb.2019.117941>.
- [49] V. Deeratrakul, N. Yigit, G. Rupprechter, P. Kongkachuichay, The roles of nitrogen species on graphene aerogel supported Cu–Zn as efficient catalysts for CO<sub>2</sub> hydrogenation to methanol, *Appl. Catal. A: Gen.* 580 (2019) 46–52, <https://doi.org/10.1016/j.apcata.2019.04.030>.
- [50] T. Liu, X. Hong, G. Liu, In situ generation of the Cu@3D-ZrOx framework catalyst for selective methanol synthesis from CO<sub>2</sub>/H<sub>2</sub>, *ACS Catal.* 10 (1) (2020) 93–102, <https://doi.org/10.1021/acscatal.9b03738>.
- [51] S. Li, L. Guo, T. Ishihara, Hydrogenation of CO<sub>2</sub> to methanol over Cu/AlCeO catalyst, *Catal. Today* 339 (2020) 352–361, <https://doi.org/10.1016/j.cattod.2019.01.015>.
- [52] B. Xie, R.J. Wong, T.H. Tan, M. Higham, E.K. Gibson, D. Decarolis, J. Callison, K.-F. Aguey-Zinsou, M. Bowker, C.R.A. Catlow, J. Scott, R. Amal, Synergistic ultraviolet and visible light photo-activation enables intensified low-temperature methanol synthesis over copper/zinc oxide/alumina, *Nat. Commun.* 11 (1) (2020) 1615, <https://doi.org/10.1038/s41467-020-15445-z>.
- [53] M.C. Biesinger, Advanced analysis of copper X-ray photoelectron spectra, *Surf. Interface Anal.* 49 (13) (2017) 1325–1334, <https://doi.org/10.1002/sia.6239>.
- [54] W. Shan, F. Liu, H. He, X. Shi, C. Zhang, Novel cerium–tungsten mixed oxide catalyst for the selective catalytic reduction of NOx with NH<sub>3</sub>, *Chem. Commun.* 47 (28) (2011) 8046–8048, <https://doi.org/10.1039/C1CC12168E>.
- [55] L. Chen, J. Li, W. Ablikim, J. Wang, H. Chang, L. Ma, J. Xu, M. Ge, H. Arandiyani, CeO<sub>2</sub>–WO<sub>3</sub> mixed oxides for the selective catalytic reduction of NOx by NH<sub>3</sub> over a wide temperature range, *Catal. Lett.* 141 (12) (2011) 1859–1864, <https://doi.org/10.1007/s10562-011-0701-4>.
- [56] P. Kumar, P. With, V.C. Srivastava, R. Gläser, I.M. Mishra, Efficient ceria-zirconium oxide catalyst for carbon dioxide conversions: characterization, catalytic activity and thermodynamic study, *J. Alloy. Compd.* 696 (2017) 718–726, <https://doi.org/10.1016/j.jallcom.2016.10.293>.
- [57] B. Liu, C. Li, G. Zhang, X. Yao, S.S.C. Chuang, Z. Li, Oxygen vacancy promoting dimethyl carbonate synthesis from CO<sub>2</sub> and methanol over Zr-doped CeO<sub>2</sub> nanorods, *ACS Catal.* 8 (11) (2018) 10446–10456, <https://doi.org/10.1021/acscatal.8b00415>.
- [58] Z. Fu, Y. Zhong, Y. Yu, L. Long, M. Xiao, D. Han, S. Wang, Y. Meng, TiO<sub>2</sub>-doped CeO<sub>2</sub> nanorod catalyst for direct conversion of CO<sub>2</sub> and CH<sub>3</sub>OH to dimethyl carbonate: catalytic performance and kinetic study, *ACS Omega* 3 (1) (2018) 198–207, <https://doi.org/10.1021/acsomega.7b01475>.
- [59] L. Lin, S. Yao, Z. Liu, F. Zhang, N. Li, D. Vovchok, A. Martínez-Arias, R. Castañeda, J. Lin, S.D. Senanayake, D. Su, D. Ma, J.A. Rodríguez, In situ characterization of Cu/CeO<sub>2</sub> nanocatalysts for CO<sub>2</sub> hydrogenation: morphological effects of nanostructured ceria on the catalytic activity, *J. Phys. Chem. C* 122 (24) (2018) 12934–12943, <https://doi.org/10.1021/acs.jpcc.8b00415>.
- [60] B.M. Reddy, A. Khan, Y. Yamada, T. Kobayashi, S. Loridant, J.-C. Volta, Surface characterization of CeO<sub>2</sub>/SiO<sub>2</sub> and V<sub>2</sub>O<sub>5</sub>/CeO<sub>2</sub>/SiO<sub>2</sub> catalysts by Raman, XPS, and other techniques, *J. Phys. Chem. B* 106 (42) (2002) 10964–10972, <https://doi.org/10.1021/jp021195v>.
- [61] M. Lykaki, E. Pachatouridou, S.A.C. Carabineiro, E. Iliopoulou, C. Andriopoulou, N. Kallithrakas-Kontos, S. Boghosian, M. Konsolakis, Ceria nanoparticles shape effects on the structural defects and surface chemistry: implications in CO oxidation by Cu/CeO<sub>2</sub> catalysts, *Appl. Catal. B: Environ.* 230 (2018) 18–28, <https://doi.org/10.1016/j.apcatb.2018.02.035>.
- [62] Y. Peng, K. Li, J. Li, Identification of the active sites on CeO<sub>2</sub>–WO<sub>3</sub> catalysts for SCR of NOx with NH<sub>3</sub>: an in situ IR and Raman spectroscopy study, *Appl. Catal. B: Environ.* 140–141 (2013) 483–492, <https://doi.org/10.1016/j.apcatb.2013.04.043>.
- [63] A. Sepúlveda-Escribano, F. Coloma, F. Rodríguez-Reinoso, Promoting effect of ceria on the gas phase hydrogenation of crotonaldehyde over platinum catalysts, *J. Catal.* 178 (2) (1998) 649–657, <https://doi.org/10.1006/jcat.1998.2199>.
- [64] G.N. Vayssilov, M. Mihaylov, P. Petkov St, K.I. Hadjiivanov, K.M. Neyman, Reassignment of the vibrational spectra of carbonates, formates, and related surface species on ceria: a combined density functional and infrared spectroscopy investigation, *J. Phys. Chem. C* 115 (47) (2011) 23435–23454, <https://doi.org/10.1021/jp208050a>.
- [65] P. Bera, A.L. Cámara, A. Hornés, A. Martínez-Arias, Comparative in situ DRIFTS-MS study of 12CO- and 13CO-TPR on CuO/CeO<sub>2</sub> catalyst, *J. Phys. Chem. C* 113 (24) (2009) 10689–10695, <https://doi.org/10.1021/jp9020504>.
- [66] M. Zhu, P. Tian, R. Kurtz, T. Lunkenbein, J. Xu, R. Schlögl, I.E. Wachs, Y.-F. Han, Strong metal–support interactions between copper and iron oxide during the high-temperature water-gas shift reaction, *Angew. Chem.* 131 (27) (2019) 9181–9185, <https://doi.org/10.1002/ange.201903298>.
- [67] D. Schweke, S. Zalkind, S. Attia, J. Bloch, The interaction of CO<sub>2</sub> with CeO<sub>2</sub> powder explored by correlating adsorption and thermal desorption analyses, *J. Phys. Chem. C* 122 (18) (2018) 9947–9957, <https://doi.org/10.1021/acs.jpcc.8b01299>.
- [68] R. Koppelent, J.A. vanBokhoven, J. Szlachetko, J. Edebeli, C. Paun, M. Nachttegaal, O.V. Safonova, Catalytically active and spectator Ce<sup>3+</sup> in ceria-supported metal catalysts, *Angew. Chem.* 127 (30) (2015) 8852–8855, <https://doi.org/10.1002/ange.201503022>.
- [69] A.I. Frenkel, A. Yevick, C. Cooper, R. Vasic, Modeling the structure and composition of nanoparticles by extended X-ray absorption fine-structure spectroscopy, *Annu. Rev. Anal. Chem.* 4 (1) (2011) 23–39, <https://doi.org/10.1146/annurev-anchem-061010-113906>.
- [70] Y. Lykhach, T. Staudt, R. Streber, M.P.A. Lorenz, A. Bayer, H.-P. Steinrück, J. Libuda, CO<sub>2</sub> activation on single crystal based ceria and magnesia/ceria model catalysts, *Eur. Phys. J. B* 75 (1) (2010) 89–100, <https://doi.org/10.1140/epjb/e2010-00110-x>.
- [71] Z. Li, K. Werner, L. Chen, A. Jia, K. Qian, J.-Q. Zhong, R. You, L. Wu, L. Zhang, H. Pan, X.-P. Wu, X.-Q. Gong, S. Shaikhutdinov, W. Huang, H.-J. Freund, Interaction of hydrogen with ceria: hydroxylation, reduction, and hydride formation on the surface and in the bulk, *Chem. – Eur. J.* 27 (16) (2021) 5268–5276, <https://doi.org/10.1002/chem.202005374>.
- [72] J.I. Flége, B. Kaemena, J. Höcker, F. Bertram, J. Wollschläger, T. Schmidt, J. Falta, Ultrathin, epitaxial cerium dioxide on silicon, *Appl. Phys. Lett.* 104 (13) (2014), 131604, <https://doi.org/10.1063/1.4870585>.
- [73] Y. Yang, D. Mei, C.H.F. Peden, C.T. Campbell, C.A. Mims, Surface-bound intermediates in low-temperature methanol synthesis on copper: participants and spectators, *ACS Catal.* 5 (12) (2015) 7328–7337, <https://doi.org/10.1021/acscatal.5b02060>.
- [74] S. Kattel, B. Yan, Y. Yang, J.G. Chen, P. Liu, Optimizing binding energies of key intermediates for CO<sub>2</sub> hydrogenation to methanol over oxide-supported copper, *J. Am. Chem. Soc.* 138 (38) (2016) 12440–12450, <https://doi.org/10.1021/jacs.6b05791>.
- [75] A. Karelavic, G. Galdames, J.C. Medina, C. Yévenes, Y. Barra, R. Jiménez, Mechanism and structure sensitivity of methanol synthesis from CO<sub>2</sub> over SiO<sub>2</sub>-supported Cu nanoparticles, *J. Catal.* 369 (2019) 415–426, <https://doi.org/10.1016/j.jcat.2018.11.012>.
- [76] S.D. Senanayake, P.J. Ramírez, I. Waluyo, S. Kundu, K. Mudiyansele, Z. Liu, Z. Liu, S. Axnanda, D.J. Stacchiola, J. Evans, J.A. Rodríguez, Hydrogenation of CO<sub>2</sub> to methanol on CeOx/Cu(111) and ZnO/Cu(111) catalysts: role of the metal–oxide interface and importance of Ce<sup>3+</sup> sites, *J. Phys. Chem. C* 120 (3) (2016) 1778–1784, <https://doi.org/10.1021/acs.jpcc.5b12012>.
- [77] C. Li, Y. Sakata, T. Arai, K. Domen, K. Maruya, T. Onishi, Carbon monoxide and carbon dioxide adsorption on cerium oxide studied by Fourier-transform infrared spectroscopy. Part 1.—formation of carbonate species on dehydroxylated CeO<sub>2</sub>, at room temperature, *J. Chem. Soc., Faraday Trans. 1* 85 (4) (1989) 929–943, <https://doi.org/10.1039/F19898500929>.
- [78] C. Li, Y. Sakata, T. Arai, K. Domen, K. Maruya, T. Onishi, Adsorption of carbon monoxide and carbon dioxide on cerium oxide studied by Fourier-transform infrared spectroscopy. Part 2.—formation of formate species on partially reduced CeO<sub>2</sub> at room temperature, *J. Chem. Soc., Faraday Trans. 1* 85 (6) (1989) 1451–1461, <https://doi.org/10.1039/F19898501451>.
- [79] L.G. Appel, J.G. Eon, M. Schmal, The CO<sub>2</sub>–CeO<sub>2</sub> interaction and its role in the CeO<sub>2</sub> reactivity, *Catalysis Letters* 56 (4) (1998) 199–202, <https://doi.org/10.1023/A:1019098121432>.